

Transient surface temperatures upon the impact of a single droplet onto a heated surface in the film evaporation regime

Mahsa Ebrahim ^{a,c}, Buddha Elkenani ^a, Alfonso Ortega ^b

a Loyola Marymount University, 1 LMU Dr., Los Angeles, CA, 90045, USA

b Villanova University, 800 E Lancaster Ave., Villanova, PA, 19085, USA

c Corresponding author, mahsa.ebrahim@lmu.edu

Abstract

Single droplet impingement on a heated surface is a fundamental problem of basic interest in understanding complex phenomena in spray cooling and other applications involving heat transfer to impinging droplets. The surface temperature experiences rapid temporal gradients upon droplet impact. These temperature transients are strongly dependent on the hydrodynamic and heat transfer regimes. Experimental results are presented for the transient surface temperature in the film evaporation heat transfer regime for a broad range of impact Weber numbers, far above those have been previously studied in the evaporation regime. High-speed video was used to capture the dynamics of the impact. Intrinsic thermocouples were manufactured to measure surface temperature with sufficient temporal resolution. It was found that the hydrodynamics of the impact were not significantly affected by the surface temperature. Heat removal was found to be more effective at lower impact velocities. The maximum temperature drop occurred at the maximum spreading diameter. An analytical model was proposed to predict the transient Nusslet number of the droplet motion on the surface.

Keywords: Droplet impact, Spray Cooling, Gas-propelled, Transient

temperature

Nomenclature

c_p	specific heat, $\frac{J}{kgK}$
C	fitting constant
D	diameter, m
FF	free-falling
g	gravitational acceleration, $\frac{m}{s^2}$
GP	gas-propelled
h	heat transfer coefficient, $\frac{W}{m^2K}$
k	thermal conductivity, $\frac{W}{mK}$
L	characteristic length, $L = \frac{D_0 + \delta}{2}$, m
Nu	Nusselt number, $Nu = \frac{hD}{k}$
Pr	Prandtl number, $Pr = \frac{\nu}{\alpha}$
Ra	Rayleigh number, $Ra = \frac{\rho g L^3 \Delta T}{\nu \alpha}$
Re	Reynolds number, $Re = \frac{\rho DV}{\mu}$
T	temperature, K
t	time, s
V	velocity, $\frac{m}{s}$

We Weber number, $We = \frac{\rho DV^2}{\sigma}$

x axial coordinate, m

Greek symbols

α thermal diffusivity, $\frac{m^2}{s}$

δ liquid film thickness, m

μ dynamic viscosity, $Pa.s$

ν kinematic viscosity, $\frac{m^2}{s}$

ρ density, $\frac{kg}{m^3}$

σ surface tension, $\frac{N}{m}$

τ dimensionless time, $\tau = \frac{tV_0}{D_0}$

θ dimensionless temperature, $\theta = \frac{T-T_\infty}{T_s-T_\infty}$

ξ spreading factor, $\xi = \frac{D}{D_0}$

Subscripts

∞ ambient

0 impact condition

c characteristic

d droplet

di droplet initial

free free convection

g propellant gas

h	hydrodynamic
max	maximum
min	minimum
s	surface
sat	saturation
si	surface initial
stag	stagnation
th	thermal

1. Introduction

Single and multiple droplet impingement studies have gained significant attention due to their broad applications in plasma coating, inkjet printers, metal forming, and especially in spray cooling [1–3]. Extensive research has been performed on droplet impact at high surface temperatures, leading to the boiling and Leidenfrost regimes, and at low impact velocities. Fewer researchers have studied droplet impingement at high impact conditions in regimes with phase change [4–6]. This paper presents experimental results of single droplet impingement at moderate to high impact We numbers in the film evaporation heat transfer regime.

Considerable experimental work has been done on single droplet impingement on heated surfaces at low impact We numbers ($We < 1100$) because of practical reasons and difficulties in accelerating droplets beyond free fall limits [1, 2, 7–15]. It has been shown that the maximum spreading diameter was enhanced as impact We number increased [3, 16]. Staat et al. [8] detected splashing at higher impact We numbers (≈ 1000) or at surface temperatures above

the Leidenfrost state. For superheated surfaces, it was shown that the maximum spreading diameter of droplets scaled with the $We^{\frac{2}{5}}$ in gentle boiling and spray film boiling regimes which were distinct boiling regimes previously identified for surface temperature above the saturation [7]. Bertola [11] discovered that the Leidenfrost temperature threshold was reduced when small amounts of polymers were added to water droplets. Empirical correlations were developed to approximate the maximum spreading factor and the dimensionless droplet resident life on the surface [10]. It was observed by Liang et al. [14] that the evaporation time was not significantly affected by the impact process because the evaporation time was considerably longer than the droplet hydrodynamic time scales during impact and spreading.

Many researchers have developed phase diagrams (heat transfer regime maps) with respect to impact We number for single droplet impingement on heated surfaces [7, 8, 10, 12, 13, 17–19]. However, there are some discrepancies between these phase diagrams because they are solely based on hydrodynamic quantities and the initial surface temperature while the outcomes also depend on the thermal quantities [2, 20]. Furthermore, it was determined that We is not sufficient to fully scale the droplet impingement hydrodynamics and Re can significantly affect the physics [21, 22].

In the literature on the heat transfer of a single droplet impinging on a heated surface, the effects of impact condition on the instantaneous surface temperature have not been investigated for $We > 500$. In the majority of the investigations, only the surface temperature before the impact was considered as a parameter [1, 2, 23]. Available correlations either calculate an average surface temperature assuming two semi-infinite surfaces or they apply only to surface temperatures above the saturation temperature [9]. Thus, the problem characteristics and the unexpected temperature behavior, especially during the early stages of impact,

still remain unknown. High fidelity numerical simulations are challenging during these early impact stages, hence accurate data are crucial for validation.

This paper investigates the effects of We number ($200 < We < 6000$) on the transient surface temperature in the film evaporation heat transfer regime in which $T_s < T_{sat}$. In order to vary the impact We number over a broad range and to increase it far above that were previously studied, gas-propelled droplets (droplet acceleration through an air stream [4]) and free-falling droplets (gravitational acceleration) were studied. Multiple intrinsic thermocouples with high temporal response were manufactured following the design of Heichal et al. [24] to measure the dynamic temperature at the contact surface. A high-speed digital video camera was utilized to capture the hydrodynamics of the spreading and receding phases. The effects of impact velocity and the surface temperature on the droplet dynamics and the heat transfer were investigated. An analytical model was proposed for the transient heat transfer coefficient between the surface and the droplet.

2. Experimental Apparatus

An experimental apparatus from the prior work of the authors was modified to allow testing of both free-falling and gas-propelled droplets [4, 5]. The schematics of different parts of the experimental apparatus are shown in Figs. 1, 2, and 3. The experimental apparatus consists of (i) the droplet dispenser, (ii) the air propellant flow delivery system and flow straightener, (iii) high-speed video camera, and (iv) the heated surface with intrinsic thermocouples. Part (ii) was only utilized for the gas-propelled droplet experiments. The details of each part are as follows.

(i) *Droplet dispenser*- A pneumatic fluid dispenser (Nordson EFD Inc. Model No. 741) was utilized to generate single droplets for both free-falling and gas-

propelled experiments. The dispenser used compressed air to pressurize the distilled water supply tank in order to deliver water at 22°C to the valve which dispenses single droplets with controlled and repeatable volume. For free-falling experiments, a 23-gauge hypodermic needle was utilized to generate single droplets (3.5 ± 0.3 mm). The elevation of the dispenser could be adjusted in order to achieve different impact velocities through gravitational acceleration. For gas-propelled droplets, a 30-gauge miniature stainless steel tube was used to form a 90° bend and to insert single droplets (2.1 ± 0.2 mm) into the air stream. The dispenser was fixed and the impact velocity was varied by adjusting the flow rate of the air stream.

(ii) *Air flow delivery system and flow straightener*- Compressed air was utilized to deliver air to the dispenser and the flow straightener for the gas-propelled experiments. Pressure regulators were placed upstream to control the flow pressure to deliver a steady-state constant air flow. The volumetric flow rate and temperature were measured with a laminar flow element (Meriam LFE- Model 50MJ10) and a K-type thermocouple, respectively. The flow rate was modulated through a needle valve and directed into the flow straightener for the gas-propelled experiments. In order to generate a unidirectional flow and to minimize any disturbance in the flow that could affect the trajectory of the droplet as it traveled inside a long tube, a flow conditioning section was designed to first decelerate the air flow in a diffuser and then accelerate the flow in a nozzle. The droplets were inserted at the inlet to the converging nozzle. Further details of the flow straightener, the apparatus design, tube length, repeatability, and validation are explained in the authors' previous work [4, 5].

(iii) *High-speed video camera*- A digital high-speed camera (Vision Research, Phantom 7.1TM) with sufficient illumination was used to closely observe the

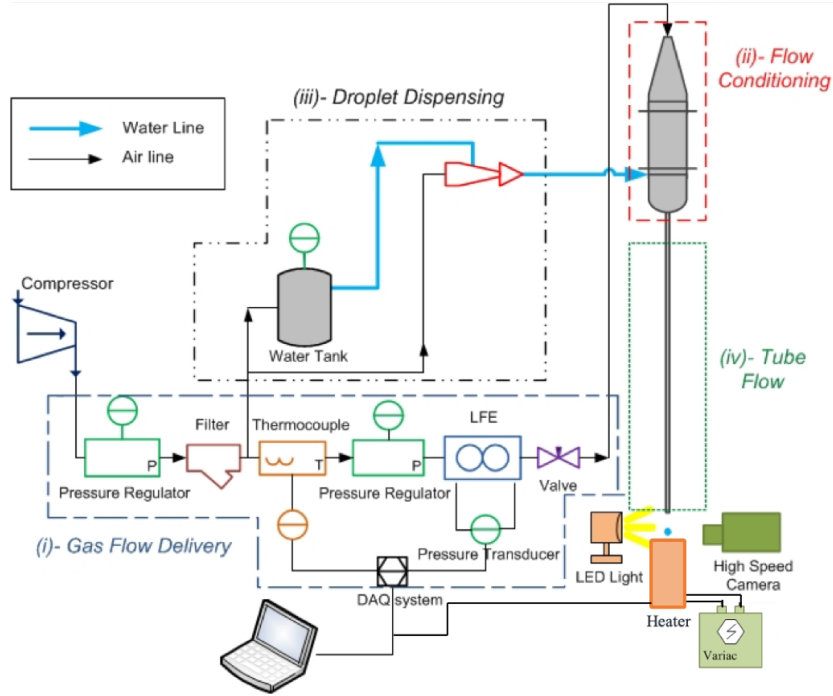


Figure 1: Schematic of the gas-propelled apparatus

spreading and receding phases by capturing the hydrodynamics at 20,000 fps with a resolution of 320×288 pixels. The droplet initial diameter, impact velocity, and its instantaneous diameter were measured using frame by frame analysis in the Phantom PCC3.3 software that was provided by the digital camera.

(iv) *The heated surface with intrinsic thermocouples-* The heater was fabricated from a copper rod (1.75" diameter, 3" length) with inserted cartridge heaters (2" length, 3/16" diameter) as seen in Fig. 3. The target surface, made of 303 stainless-steel (1.75" diameter, 0.25" thickness), was placed on top of the copper heater. Thermal paste was used to decrease the thermal resistance between the stainless-steel substrate and the heater. The technique described by Heichal et al. [24], was used to design intrinsic thermocouples that were inserted into the target surface. The stainless-steel substrate was the positive alloy of the thermocouples and constantan (40 AWG) wires, as the negative alloys were

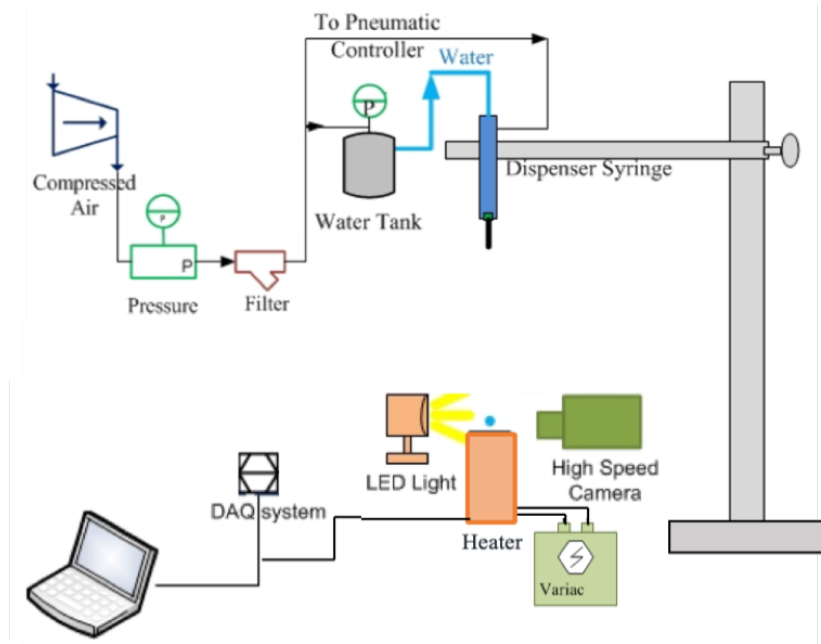


Figure 2: Schematic of the free-falling apparatus

inserted into holes that were drilled along the axis of the substrate, as shown in Fig. 3. Individual thermocouple junctions were made on the surface of the stainless-steel substrate by making electrical connections between the constantan wires and the stainless steel surface with silver ink (Micro-Tip Conductive Pen, SPI Supplies). The thermocouples were calibrated by inserting the test surface in a constant temperature chamber. Further details on the design and calibration process of the intrinsic thermocouples are described in the authors' prior work [25].

Temperature data were collected at 200 kHz using a NI-USB-6281 data acquisition system, which provides a sufficiently high temporal resolution to capture temperature variation during the spreading phase. Due to the fast rate of measurements and the nature of the intrinsic thermocouples [24], recording the surrounding noise in the measurements was inevitable. A MATLAB wavelet

de-noising function was therefore utilized to remove the unwanted surrounding noise from the measured temperature data.

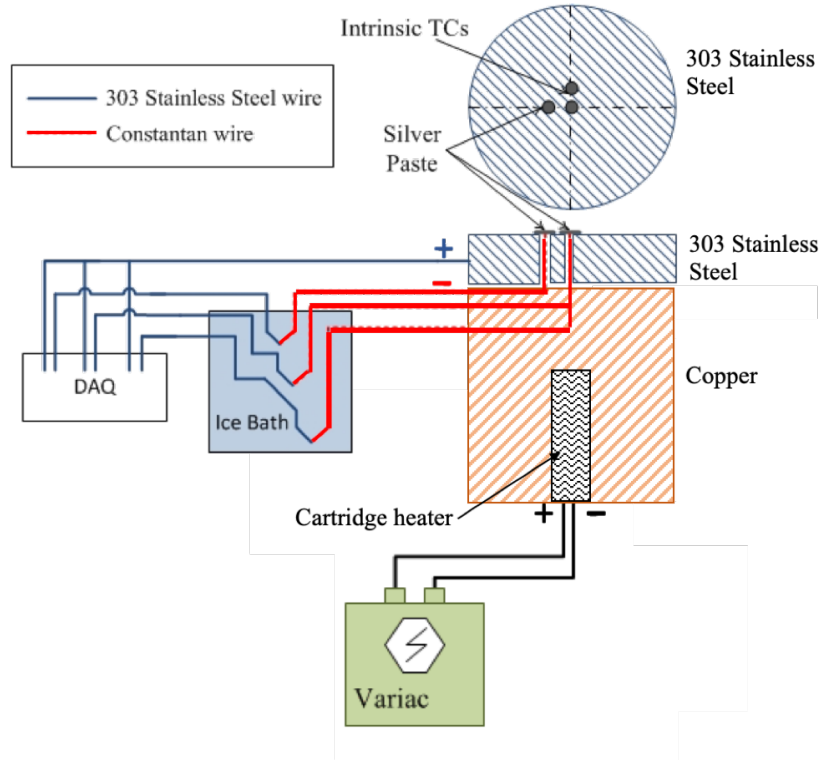


Figure 3: Schematic of heater with intrinsic thermocouples

3. Results and Discussion

Time elapsed video frames of droplet hydrodynamics after the impact are depicted in Fig. 4. It can be seen that the droplet starts to spread as it impacts the surface. The spreading phase ends and the droplet achieves its maximum spreading diameter when all its initial kinetic energy is converted into the surface tension energy and dissipated into the surface shear stress. At this moment, the surface tension energy is strong enough to reverse the flow direction towards the center and initiate the receding phase. Depending on the impact condition

and surface wettability, the receding phase could continue until the droplet either detaches from the surface and rebounds, or to oscillates in a series of spreading/receding cycles. The spreading phase is significantly faster than the receding phase and the majority of the heat is transferred during the receding phase [1, 2, 5, 18]. Previous work by the authors found that the spreading phase was not significantly affected by the propellant gas while the receding phase was delayed as the propellant gas Re number, Re_g , was increased [5].

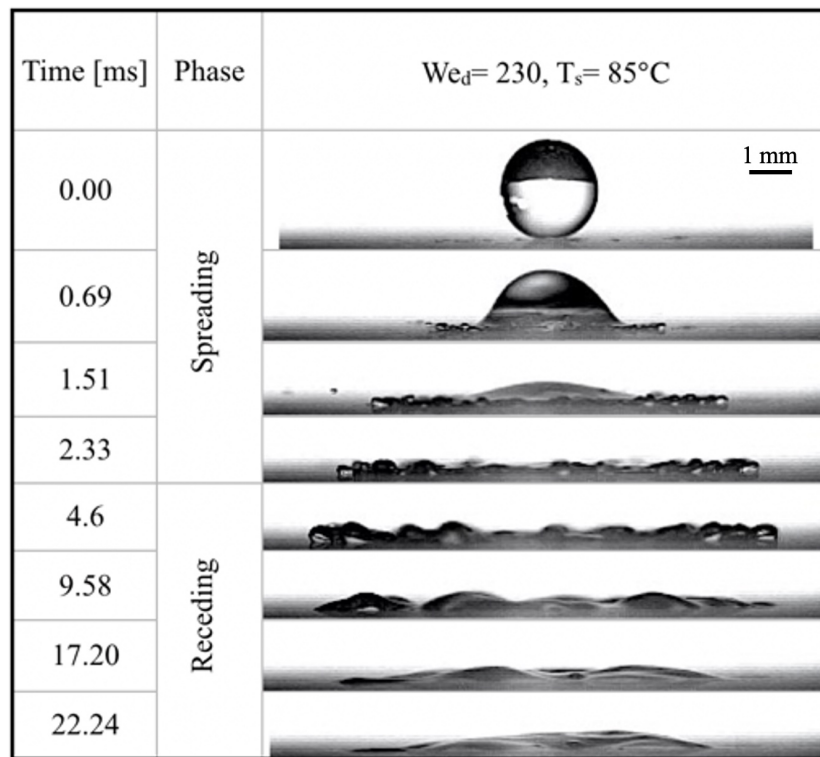


Figure 4: Time elapsed images of the droplet impact

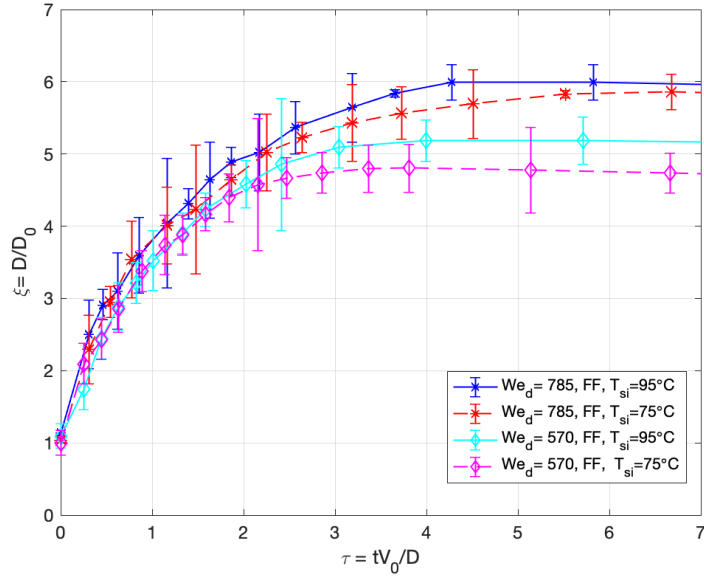
Four distinct heat transfer regimes of film evaporation, nucleation boiling, transitional boiling, and film boiling or Leidenfrost have been identified for droplet impingement on a heated surface ~~as shown in Fig. ??~~ [1, 2]. The temperature variation upon the impact, i.e., during the spreading phase and early

receding phase, in the film evaporation heat transfer regime is the focus of this study. The range of parameters tested is shown in Table 1. The hydrodynamics and heat transfer results are discussed in the following sections.

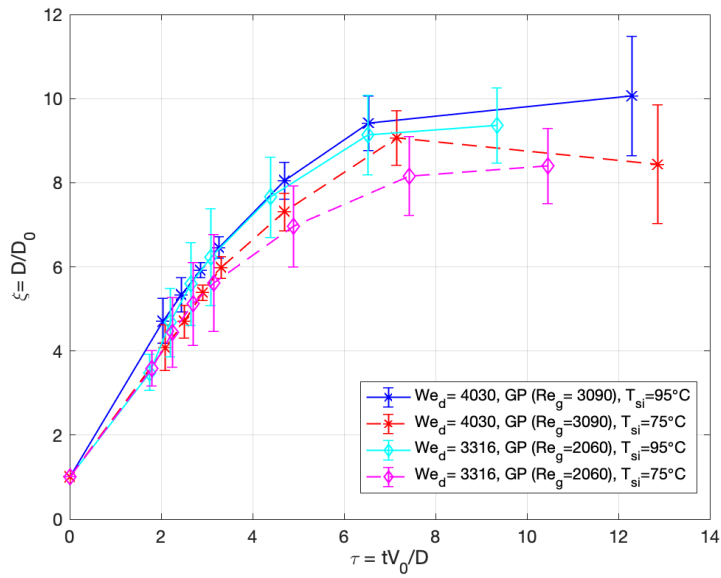
Table 1: Variation of test data

	D_0 , [mm]	V_0 , [m/s]	Re_d	We_d	Re_g	T_{si} [$^{\circ}$ C]
Min.	2.1	2.3	8500	230	0	60
Max.	3.5	13.6	34000	5540	4300	100

Hydrodynamics- The impact velocity, initial diameter, and the instantaneous droplet diameter after the impact were measured using the frame by frame analysis of high-speed videos. Each impact condition was repeated for five to ten times and ensemble averaged. The uncertainty in the measured data, **calculated as three times the standard deviation of the repeated measurements**, is indicated in the error bars shown in Fig. 5. Representative instantaneous spreading factor, $\xi = \frac{D}{D_0}$, for free-falling and gas-propelled droplets are shown in Fig. 5. It can be seen that for a given impact We_d number, the spreading factor is slightly enhanced as the surface temperature increases for both free-falling and gas-propelled impact conditions. Since the surface tension decreases at higher temperatures, the droplet spreads more at a given impact kinetic energy. The maximum spreading diameter for both free-falling and gas-propelled droplets is enhanced as We_d number increases. **Because the spreading factor is more profoundly affected by the We_d , the correlation from Diaz and Ortega [6] can still be used to predict the maximum spreading diameter in the film evaporation regime.**



(a) Free-falling



(b) Gas-propelled where Re_g represents the propellant air Re number

Figure 5: Spreading factor for different droplet impact We numbers and surface temperatures; (a)- Free-falling, (b)- Gas-propelled.

Heat transfer- Because of the uncertainty in the exact impact coordinates of the droplet, three intrinsic thermocouples were clustered closely around the expected center of the impact, as shown in Fig. 3. The temperature values from the thermocouple with the maximum temperature drop was chosen for each impact trial, considering that it was the closest thermocouple to the center of the impact. Every impact condition was repeated five to ten times and ensemble averaged. The error bars in the following Figures (6, 7, 8, and 10) **represent the uncertainty calculated as three times the standard deviation of the repeated trials before filtering the measurements in MATLAB Wavelet application.**

The non-dimensional surface temperature, $\theta = \frac{T-T_\infty}{T_{si}-T_\infty}$, at the center of the impact for free-falling droplets at a given impact condition is shown in Fig. 6. It can be seen that the temperature drops upon the impact and then increases towards the initial surface temperature, T_{si} . A closer comparison of Fig. 6 and Fig. 5a shows that the temperature drop occurs at the early stage of the spreading phase ($0 < \tau = \frac{tV_0}{D} < 10$), the lowest temperature is achieved at the maximum spreading diameter, and the temperature increase happens during the receding phase. It is also evident that θ is not significantly affected by the initial surface temperature for film evaporation regime, $T_{si} < T_{sat}$.

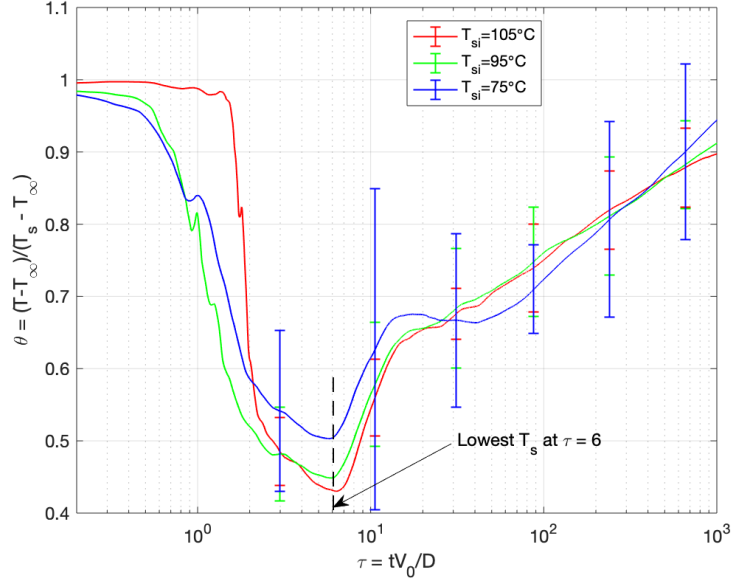
Figure 7 shows the non-dimensional surface temperature, θ , for gas propelled droplets at fixed impact conditions and different initial surface temperatures. It can be seen that the first temperature drop occurs during the spreading phase when $0 < \tau < 14$ according to Fig. 5b. For gas-propelled droplets, there is a secondary temperature drop during the receding phase. This may be hypothesized to be due to at least one secondary spreading-receding cycle at high impact We_d . Another potential mechanism for this secondary temperature drop is the propellant air because the center of the droplet may fully evaporate during the receding phase which will expose the center to the impinging air jet and its

stagnation point. Further research is needed to fully understand the driving physics of this secondary temperature drop and perhaps simultaneously observe the droplet dynamics from different angles. Similar to free-falling droplets, the initial surface temperature does not significantly affect the temperature gradients for gas-propelled droplets in film evaporation regime.

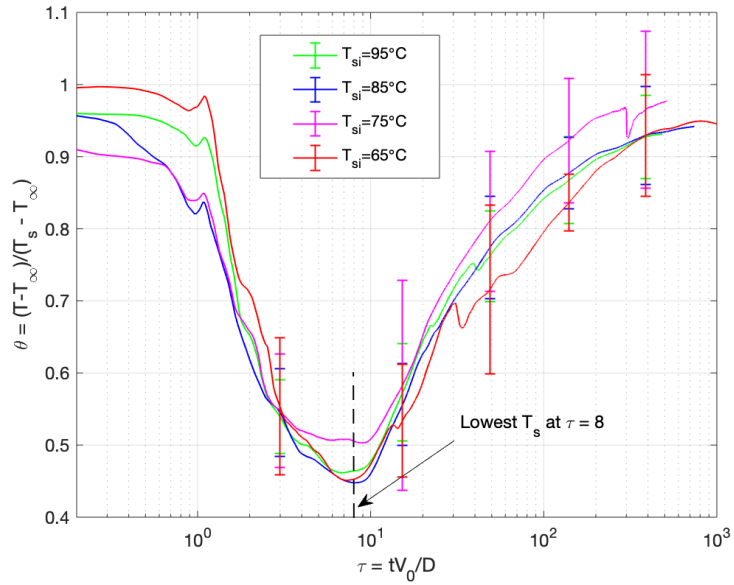
The effects of the impact We_d on the non-dimensional surface temperature, θ , at a given initial surface temperature is shown in Fig. 8. It can be seen that the We_d does not noticeably influence the surface temperature for both free-falling and gas-propelled droplets. However, it is evident that at higher impact We_d numbers or gas-propelled droplets, the maximum temperature drop is less than free-falling or low We_d conditions at all surface temperatures. This can also be deduced by the comparison of Figs. 6 and 7 and is further demonstrated in Fig. 9 in which the minimum dimensionless surface temperature, θ_{min} , is plotted versus impact We_d number. One can expect the contrary and anticipate enhanced temperature drop since at higher impact We_d numbers, the droplet spreads more rapidly and forms a thinner and larger diameter liquid film on the surface. This can be explained by the comparison of the characteristic thermal and hydrodynamic time scales [9]. At high impact We_d numbers, the thermal time scale, $\tau_{th} = \frac{\rho_s C_{ps} k_s}{h^2}$, is orders of magnitude less than the hydrodynamic time scale, $\tau_h = D_0/V_0$, and there is not enough time for heat dissipation during the spreading phase even though the contact area between the droplet and the surface is enhanced. Thus, higher impact kinetic energy does not necessarily enhance the heat transfer and the surface temperature decreases more for free-falling droplets, albeit at longer times.

Figure 9 shows that there is a secondary enhancement in the minimum dimensionless surface temperature, θ_{min} , as We_d increases in the gas-propelled impact regime. It can be speculated that this enhancement in heat transfer

is due to the propellant air flow regime. As the propellant air transitions to turbulent regime ($We_d \approx 4500$ which corresponds to $Re_g \approx 3000$), it further affects the dynamics of the impact and thus the heat removal process.

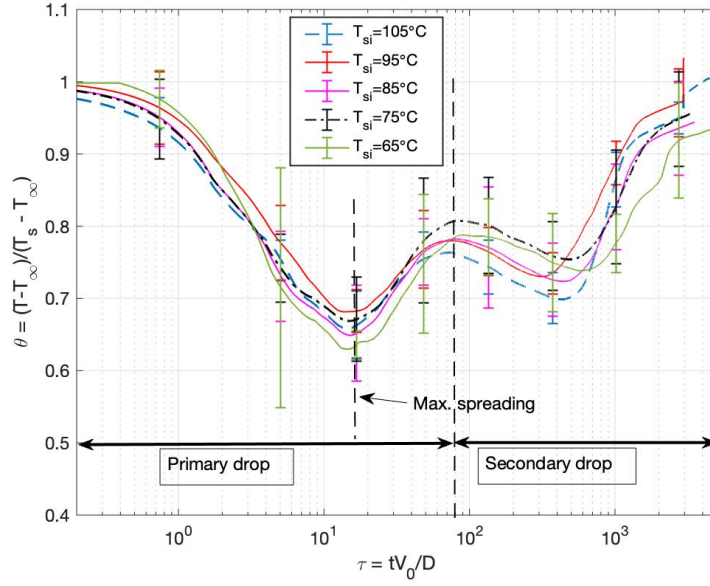


(a) Free-falling at $We_d = 230$

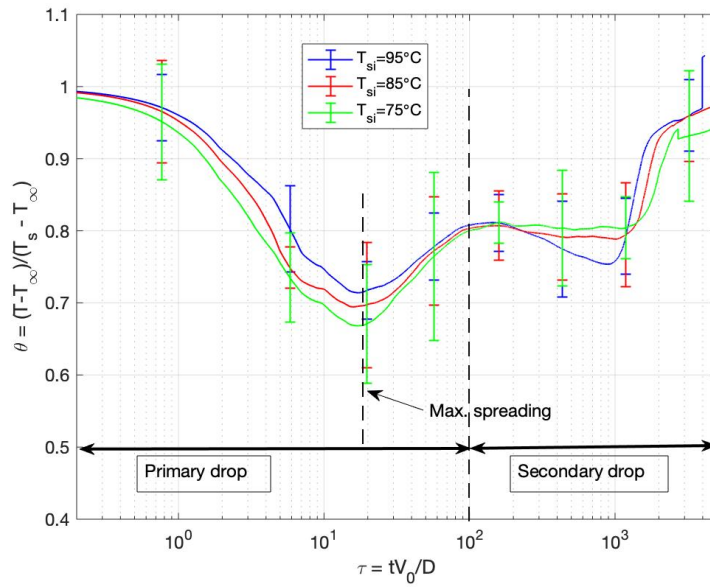


(b) Free-falling at $We_d = 600$

Figure 6: Instantaneous surface temperature at the center of the impact for a given impact condition at different surface temperatures for a free-falling droplet, (a) $We_d = 230$, (b)- $We_d = 600$.

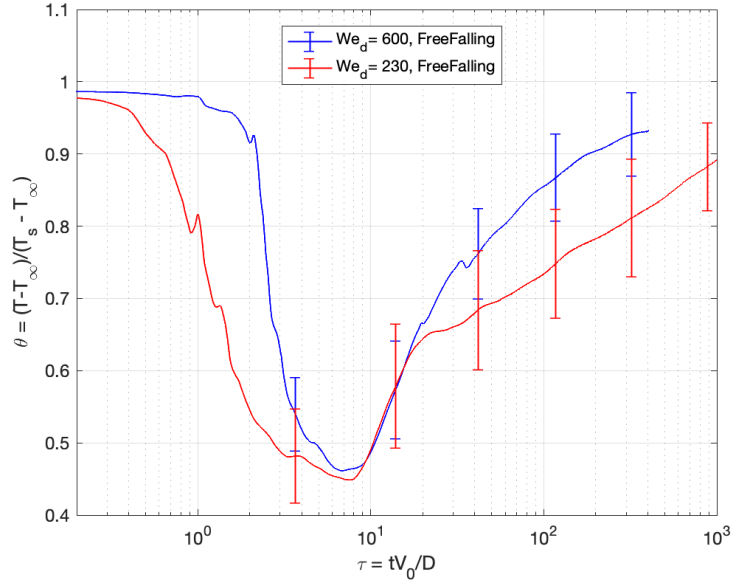


(a) Gas-propelled ($Re_g = 3090$) at $We_d = 4030$

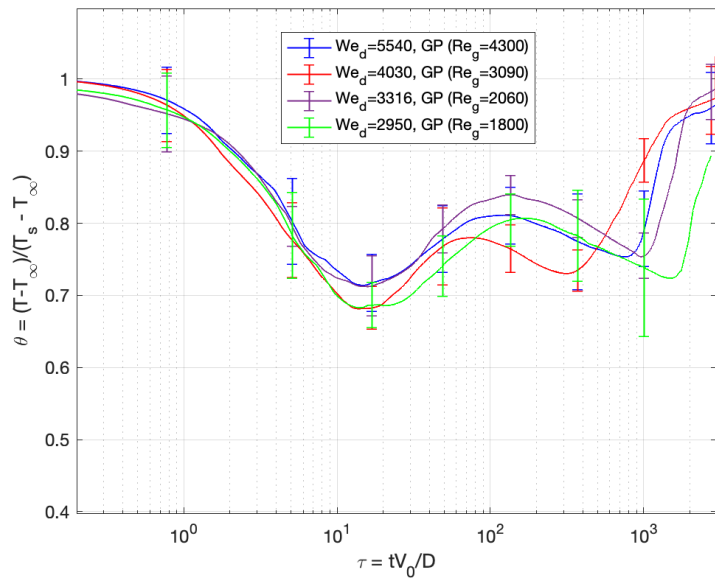


(b) Gas-propelled ($Re_g = 4300$) at $We_d = 5540$

Figure 7: Instantaneous surface temperature at the center of the impact for a given impact condition at different surface temperatures for a gas-propelled droplet where Re_g represents the propellant air Re number, (a) $We_d = 4030$, (b)- $We_d = 5560$.



(a) $T_{si} = 90^\circ C$, free-falling



(b) $T_{si} = 90^\circ C$, gas-propelled

Figure 8: Instantaneous surface temperature at the center of the impact for a given initial surface temperature at different impact conditions.

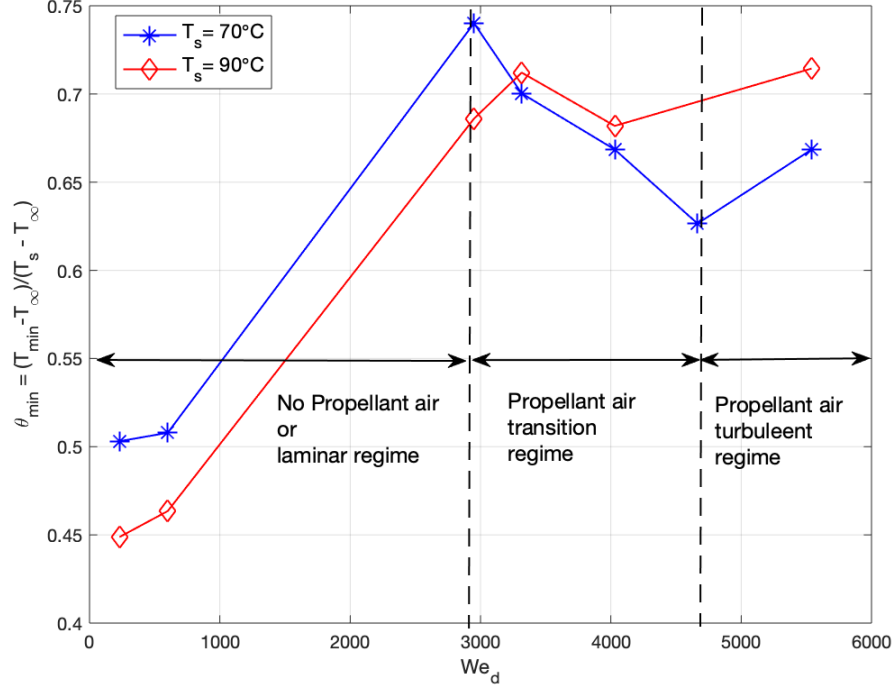


Figure 9: The minimum non-dimensional surface temperature with respect to impact We_d .

3.1. Surface temperature modeling

There are only a few analytical models that predict the surface temperature after the impact of a single droplet due to the complexity of the problem [9, 23, 26, 27]. The most widely used model was derived using the classical heat transfer problem of two semi-infinite surfaces coming to a sudden contact. In this model, the contact temperature, T_s , as given in Eq. 1, was approximated by assuming that the droplet and the surface were both semi-infinite surfaces at constant temperatures [23, 28].

$$T_s = \frac{\sqrt{\rho_d C_{p,d} k_d} T_{di} + \sqrt{\rho_s C_{p,s} k_s} T_{si}}{\sqrt{\rho_d C_{p,d} k_d} + \sqrt{\rho_s C_{p,s} k_s}} \quad (1)$$

where T_{si} and T_{di} , are the surface and droplet initial temperatures, respectively. Equation 1 is based on a constant surface boundary condition for both semi-infinite surfaces, which is not a reasonable assumption especially during the spreading phase since the surface temperature changes dramatically. Van Limbeek et al. [9] proposed to use the solution for a semi-infinite surface with convection boundary condition. The transient surface temperature at the center of impact is given as:

$$\frac{T_s - T_{sat}}{T_{si} - T_{sat}} = \exp\left(\frac{t}{\tau_{th}}\right) \operatorname{erfc}\left(\sqrt{\frac{t}{\tau_{th}}}\right) \quad (2)$$

where τ_{th} is the characteristic thermal time scale and is given as $\tau_{th} = \frac{\rho_s C_{ps} k_s}{h^2}$. They empirically calculated $h = 8 \times 10^4 \text{W/m}^2\text{K}$ by fitting the experimental data for a millimeter size droplet impacting a heated surface at low impact velocities and surface temperatures above the saturation temperature of the droplet (nucleate and transitional boiling heat transfer regimes). However, this solution predicts a surface temperature that continuously decreases, even during the receding phase. This is due to the assumption that h remains constant at all hydrodynamic phases and that the droplet remains at ambient temperature.

We propose a model in which the surface is considered to be a semi-infinite surface; instead of using an empirical and constant heat transfer coefficient, a model is developed to directly calculate it. Moreover, a transient lumped capacitance model is considered for the droplet temperature instead of assuming that the droplet remains at ambient temperature.

The convective heat transfer coefficient is approximated by modeling the droplet impact process as a finite transient impinging liquid jet that impinges on the surface for a short period of time and transitions to a static liquid film in contact with the surface. Therefore, a combination of the stagnation Nusselt number, $\text{Nu}_{stag.}$, for a continuous circular impinging jet and a free convection

Nusselt number, Nu_{free} , was considered. A correlation for the Nusselt number of the droplet impact was developed by exponentially transitioning the stagnation Nu number of a circular jet, $\text{Nu}_{stag.}$, into a free convection Nu number, Nu_{free} , as follows:

$$\text{Nu}(t) = C_1 \text{Re}_d^{0.5} \text{Pr}_d^{0.4} \exp\left(-\frac{t}{C_3 \tau_c}\right) + C_2 \text{Ra}_d^{0.25} \quad (3)$$

where the coefficient of the exponential term in Eq. 3 is the correlation for the stagnation Nu number of an impinging jet and the second term is the correlation for the free convection Nu number [28, 29]. The transitional time constant, τ_c , in Eq. 3 was determined by estimating the time that takes for the initial kinetic energy of the droplet to convert to surface tension energy as $\tau_c = \sqrt{\frac{\rho_d D_0^3}{3\sigma_d}}$. The constants of C_1 , C_2 , and C_3 are listed in Table 2.

Table 2: Constants of Eq. 3

Impact regime	C_1	C_2	C_3
Free-falling	1.0	1.0	1.2
Gas-propelled	0.4	1.0	0.5

The initial droplet diameter, D_0 , was considered as the characteristic length scale to calculate the droplet Re number, $\text{Re}_d = \frac{\rho_d D_0 V_0}{\mu_d}$. The droplet hydrodynamics and consequently the liquid film thickness at the center, dramatically change upon the impact towards the receding phase. Thus, another characteristic length scale, L , was proposed as the average of the initial diameter, D_0 , and the minimum film thickness, δ , that is formed by the droplet during the spreading phase for the calculation of droplet Rayleigh number, $\text{Ra}_d = \frac{\rho_d g L^3 (T_{si} - T_\infty)}{\nu_d \alpha_d}$ and the transient heat transfer coefficient $h(t) = \frac{\text{Nu}(t) k_d}{L}$. This film thickness, δ was obtained by applying the conservation of mass and using the previously developed ad-hoc model for maximum spreading factor [6], $\xi_{max} = \frac{D_{max}}{D_0}$, as

follows:

$$\frac{D_{max}}{D_0} = \sqrt{\frac{We_d + We_g + 12}{3(1 - \cos\theta) + \frac{4We_d}{\sqrt{Re_d}}}} \quad (4)$$

$$\delta = \frac{2}{3} \frac{D_0^3}{D_{max}^2} \quad (5)$$

The evaporated mass was assumed negligible in the calculation of minimum liquid thickness because the majority of the evaporation occurs at the end of receding phase [1].

The heat diffusion equation for the temperature distribution inside a semi-infinite surface is as follows:

$$\frac{\partial^2 T_s}{\partial x^2} = \frac{1}{\alpha_s} \frac{\partial T_s}{\partial t} \quad (6)$$

where the initial and boundary conditions are given as:

$$\left\{ \begin{array}{l} T_s(x, 0) = T_{si}, \end{array} \right. \quad (7a)$$

$$\left\{ \begin{array}{l} -k_s \frac{\partial T_s(0, t)}{\partial x} = h(t) [T_s(0, t) - T_d(t)], \end{array} \right. \quad (7b)$$

$$\left\{ \begin{array}{l} T_s(\infty, t) = T_{si} \end{array} \right. \quad (7c)$$

Droplet transient temperature is given as

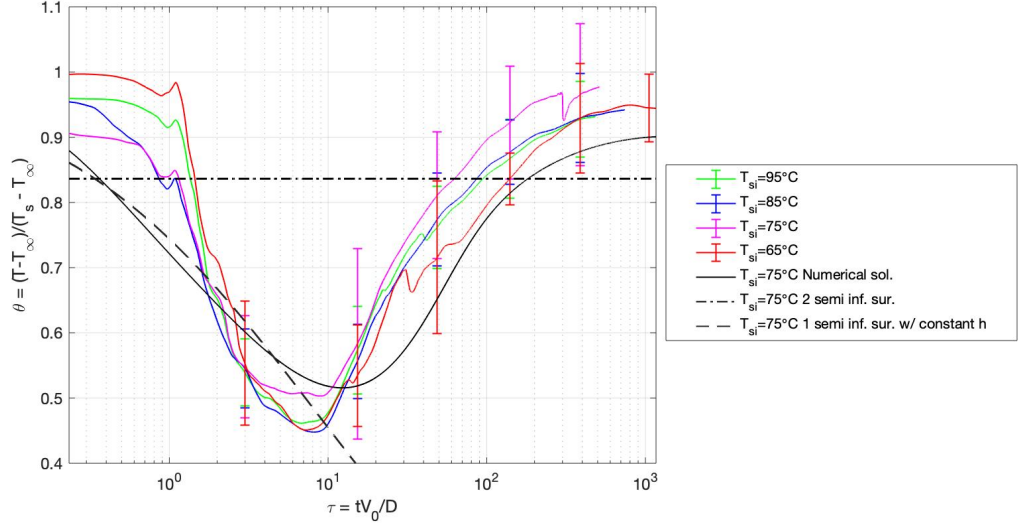
$$h(t) (T_s(0, t) - T_d(t)) - h_0 (T_d(t) - T_\infty) = (\rho_d C_{p,d} \delta) \frac{\partial T_d}{\partial t} \quad (8)$$

where the droplet initial condition is $T_d(0) = T_\infty$ and h_0 is a constant heat transfer coefficient of the ambient air. Equation. 6 is coupled with Eq. 8 through its boundary condition and therefore this system of differential equations were solved numerically.

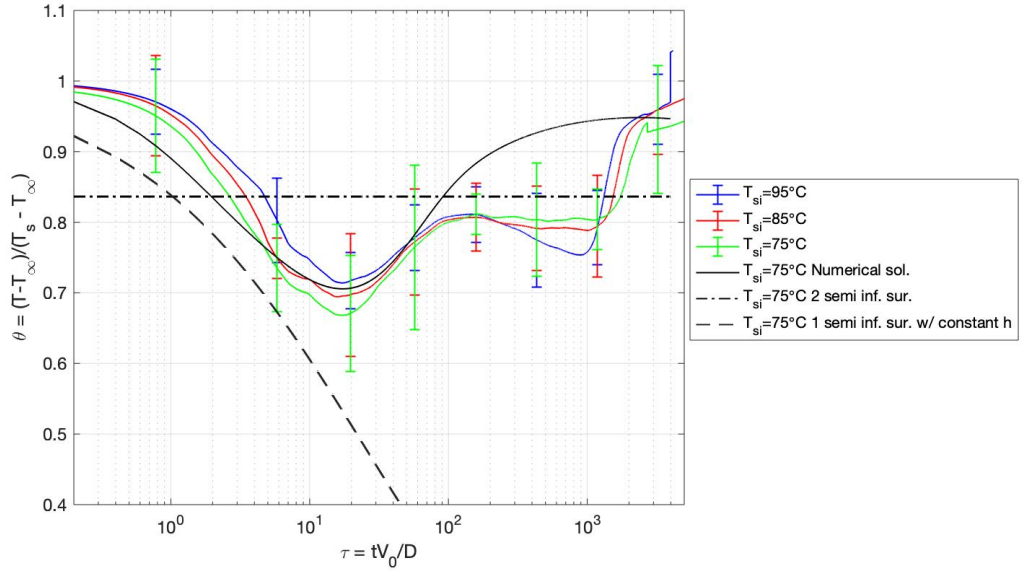
The instantaneous surface temperature at the center of the impact obtained from the numerical solution is shown in Fig. 10 for both free-falling and gas-propelled droplets and is compared with the experimental data, Eq. 1, and Eq. 2.

It can be seen in Fig. 10 that the proposed model predicts the magnitude and the time dependency of the surface temperature for free-falling droplets within $\pm 30\%$ and $\pm 10\%$, respectively. For gas-propelled droplets, the model successfully predicts the transient temperature during the primary drop phase; however, it cannot capture the physics of the secondary temperature drop.

The data comparison in Fig. 10 also reveals that the solution for two semi-infinite surfaces (Eq. 1) is a simplified method to reasonably estimate the time-averaged surface temperature at the center of the impact. However, the solution of a semi-infinite surface with a constant convective heat transfer coefficient and constant droplet temperature fails to predict the transient surface temperature as the surface continues to cool until it achieves thermal equilibrium with the droplet.



(a) Free-falling, $We_d = 600$



(b) Gas-propelled ($Re_g = 4300$), $We_d = 5540$

Figure 10: Instantaneous surface temperature at the center of the impact compared to solutions from Eq. 1 (dash-dotted line), Eq. 6 (black solid line), and Eq. 2 (dashed line).

4. Conclusions

The hydrodynamics and heat transfer of a single droplet impinging onto a dry heated surface were experimentally investigated for a broad range of impact We numbers ($200 < We_d < 6000$) in the film evaporation heat transfer regime ($T_s < T_{sat.}$). The experimental apparatus was designed in such a way that droplet impact under gravitational acceleration (free-falling) as well as further acceleration gained through an air stream (gas-propelled) can be examined. Special attention was made to the spreading phase and early receding phases in which the surface temperature experienced dramatic gradients. The following conclusions can be drawn from the investigation:

- The maximum spreading diameter was enhanced as the impact We_d was increased.
- The spreading factor, $\frac{D}{D_0}$, was not considerably affected by the surface temperature in the film evaporation heat transfer regime.
- Although droplet impingement at higher impact velocities creates a larger contact area with the surface, free-falling droplets (lower impact velocities) are more effective in heat removal during the early impact and spreading phase.
- To more effectively remove heat, the characteristic thermal time scale, τ_{th} , should be equal to or an order of magnitude smaller than the hydrodynamic time scale, τ_{hyd} .
- A correlation was proposed for the transient Nu number of the droplet motion on the surface by modeling the droplet motion as a finite impinging jet that transitions to a quiescent liquid film.

- The instantaneous surface temperature at the center of the impact can be approximated by numerically solving a semi-infinite surface that is coupled with a lumped capacitance model for the droplet and using a newly proposed transient Nu number correlation.

5. Acknowledgment

This work was supported by funding from the James R. Birle Endowment to the senior author (Prof. Alfonso Ortega). We acknowledge the contributions of our student research assistants Videhi Orugani, Theresa Siri, Joshua Amurao, and Matthew Eckles in the post-processing of the experimental data.

References

- [1] G. T. Liang, I. Mudawar, Review of drop impact on heated walls, *International Journal of Heat and Mass Transfer* 106 (2017) 103–126. doi: 10.1016/j.ijheatmasstransfer.2016.10.031.
URL <GotoISI>://WOS:000393015000010
- [2] J. Breitenbach, I. V. Roisman, C. Tropea, From drop impact physics to spray cooling models: a critical review, *Experiments in Fluids* 59 (3) (2018) 55.
- [3] A. L. Yarin, Drop impact dynamics: Splashing, spreading, receding, bouncing, *Annual Review of Fluid Mechanics* 38 (2006) 159–192. doi: 10.1146/annurev.fluid.38.050304.092144.
URL <GotoISI>://WOS:000235373900007
- [4] M. Ebrahim, A. Ortega, An experimental technique for accelerating a single liquid droplet to high impact velocities against a solid target surface using a propellant gas, *Experimental Thermal and Fluid Science* 81 (2017) 202–208. doi:10.1016/j.expthermflusci.2016.10.019.
URL <GotoISI>://WOS:000389087800017
- [5] M. Ebrahim, A. Ortega, Identification of the impact regimes of a liquid droplet propelled by a gas stream impinging onto a dry surface at moderate to high weber number, *Experimental Thermal and Fluid Science* 80 (2017) 168 – 180. doi:https://doi.org/10.1016/j.expthermflusci.2016.08.019.
URL <http://www.sciencedirect.com/science/article/pii/S0894177716302242>
- [6] A. J. Diaz, A. Ortega, Gas-Assisted Droplet Impact on a Solid Surface, *Journal of Fluids Engineering* 138 (8), 081104 (05 2016). arXiv:

https://asmedigitalcollection.asme.org/fluidsengineering/article-pdf/138/8/081104/6196666/fe_138_08_081104.pdf,
doi:10.1115/1.4033025.
URL <https://doi.org/10.1115/1.4033025>

- [7] T. Tran, H. J. J. Staat, A. Prosperetti, C. Sun, D. Lohse, Drop impact on superheated surfaces, *Phys. Rev. Lett.* 108 (2012) 036101. doi:10.1103/PhysRevLett.108.036101.
URL <https://link.aps.org/doi/10.1103/PhysRevLett.108.036101>
- [8] H. J. Staat, T. Tran, B. Geerdink, G. Riboux, C. Sun, J. M. Gordillo, D. Lohse, Phase diagram for droplet impact on superheated surfaces, *Journal of fluid mechanics* 779 (2015).
- [9] M. A. van Limbeek, M. Shirota, P. Sleutel, C. Sun, A. Prosperetti, D. Lohse, Vapour cooling of poorly conducting hot substrates increases the dynamic leidenfrost temperature, *International journal of heat and mass transfer* 97 (2016) 101–109.
- [10] G. Liang, S. Shen, Y. Guo, J. Zhang, Boiling from liquid drops impact on a heated wall, *International journal of heat and mass transfer* 100 (2016) 48–57.
- [11] V. Bertola, Drop impact on a hot surface: effect of a polymer additive, *Experiments in fluids* 37 (5) (2004) 653–664.
- [12] V. Bertola, An impact regime map for water drops impacting on heated surfaces, *International Journal of Heat and Mass Transfer* 85 (2015) 430–437.
- [13] H. Nair, H. J. Staat, T. Tran, A. van Houselt, A. Prosperetti, D. Lohse,

- C. Sun, The leidenfrost temperature increase for impacting droplets on carbon-nanofiber surfaces, *Soft matter* 10 (13) (2014) 2102–2109.
- [14] G. Liang, X. Mu, Y. Guo, S. Shen, S. Quan, J. Zhang, Contact vaporization of an impacting drop on heated surfaces, *Experimental Thermal and Fluid Science* 74 (C) (2016) 73–80. doi:10.1016/j.expthermflusci.2015.11.027.
- [15] S. Chandra, C. Avedisian, On the collision of a droplet with a solid surface, *Proceedings of the Royal Society of London. Series A: Mathematical and Physical Sciences* 432 (1991) 13 – 41.
- [16] S. Sikalo, M. Marengo, C. Tropea, E. Ganic, Analysis of impact of droplets on horizontal surfaces, *Experimental Thermal and Fluid Science* 25 (7) (2002) 503 – 510, international Thermal Science Seminar. doi:https://doi.org/10.1016/S0894-1777(01)00109-1.
URL <http://www.sciencedirect.com/science/article/pii/S0894177701001091>
- [17] M. Shirota, M. A. van Limbeek, C. Sun, A. Prosperetti, D. Lohse, Dynamic leidenfrost effect: relevant time and length scales, *Physical review letters* 116 (6) (2016) 064501.
- [18] J. D. Bernardin, C. J. Stebbins, I. Mudawar, Mapping of impact and heat transfer regimes of water drops impinging on a polished surface, *International Journal of Heat and Mass Transfer* 40 (2) (1997) 247–267.
- [19] M. Khavari, C. Sun, D. Lohse, T. Tran, Fingering patterns during droplet impact on heated surfaces, *Soft matter* 11 (17) (2015) 3298–3303.
- [20] I. Roisman, J. Breitenbach, C. Tropea, Thermal atomisation of a liquid

- drop after impact onto a hot substrate, *Journal of Fluid Mechanics* 842 (2018) 87–101.
- [21] M. Ebrahim, A. Ortega, N. Delbosc, M. C. T. Wilson, J. L. Summers, Simulation of the spreading of a gas-propelled micro-droplet upon impact on a dry surface using a lattice-boltzmann approach, *Physics of Fluids* 29 (7) (2017) 072104. arXiv:<https://doi.org/10.1063/1.4989546>, doi: 10.1063/1.4989546.
URL <https://doi.org/10.1063/1.4989546>
- [22] G. Castanet, O. Caballina, F. Lemoine, Drop spreading at the impact in the leidenfrost boiling, *Physics of Fluids* 27 (6) (2015) 063302.
- [23] M. Seki, H. Kawamura, K. Sanokawa, Transient temperature profile of a hot wall due to an impinging liquid droplet, *ASME Journal of Heat Transfer* (1978).
- [24] Y. Heichal, S. Chandra, E. Bordatchev, A fast-response thin film thermocouple to measure rapid surface temperature changes, *Experimental Thermal and Fluid Science* 30 (2) (2005) 153 – 159. doi:<https://doi.org/10.1016/j.expthermflusci.2005.05.004>.
URL <http://www.sciencedirect.com/science/article/pii/S0894177705000774>
- [25] V. Oruganti, J. Amurao, M. Ebrahim, A. Ortega, An experimental study of a single droplet impacting onto a heated surface at high impact weber numbers, in: 2019 18th IEEE Intersociety Conference on Thermal and Thermomechanical Phenomena in Electronic Systems (ITherm), 2019, pp. 342–347.
- [26] M. A. J. van Limbeek, M. H. Klein Schaarsberg, B. Sobac, A. Rednikov, C. Sun, P. Colinet, D. Lohse, Leidenfrost drops cooling surfaces: theory

and interferometric measurement, *Journal of Fluid Mechanics* 827 (2017) 614–639. doi:10.1017/jfm.2017.425.

- [27] R. Wu, O. Lamini, C. Zhao, Leidenfrost temperature: Surface thermal diffusivity and effusivity effect, *International Journal of Heat and Mass Transfer* 168 (2021) 120892. doi:<https://doi.org/10.1016/j.ijheatmasstransfer.2020.120892>.

URL <https://www.sciencedirect.com/science/article/pii/S0017931020338242>

- [28] T. L. B. Frank P. Incropera, David P. DeWitt, A. S. Lavine, *Fundamentals of Heat and Mass Transfer*, 8th Edition, Wiley, 2017.

- [29] T. Persoons, A. McGuinn, D. B. Murray, A general correlation for the stagnation point nusselt number of an axisymmetric impinging synthetic jet, *International Journal of Heat and Mass Transfer* 54 (17) (2011) 3900–3908. doi:<https://doi.org/10.1016/j.ijheatmasstransfer.2011.04.037>.

URL <https://www.sciencedirect.com/science/article/pii/S0017931011002584>